CGU HS Committee on River Ice Processes and the Environment
13th Workshop on the Hydraulics of Ice Covered Rivers
Hanover, NH, September15-16, 2005

USE OF MILLIMETER-WAVE FM-CW RADAR TO PROFILE RIVER ICE THICKNESS

Norbert E. Yankielun
ERDC – Cold Regions Research and Engineering Laboratory (CRREL)
72 Lyme Road, Hanover, New Hampshire 03755
norbert@crrel.usace.army.mil

Michael G. Ferrick
ERDC – Cold Regions Research and Engineering Laboratory (CRREL)
72 Lyme Road, Hanover, New Hampshire 03755
Michael.G.Ferrick@erdc.usace.army.mil

Samantha H. Feakins
California Institute of Technology
feakins@caltech.edu

Abstract

The use of radar to profile river ice thickness and monitor ice dynamics enables assessment of the flood hazard, the availability of water resources, the load bearing capacity the ice, as well as the potential for bridge damage and environmental impacts caused by a breakup. Advantages of radar data are their independence from manual control, visual observations or weather conditions. We suspended a millimeter-wave (MMW) frequency modulated-continuous wave (FM-CW) radar vertically over the Connecticut River from a bridge near Cornish, NH., and obtained range measurements to the ice and water surfaces below. The Ka-band (26.5-40 GHz) radar, with a spatial resolution of approximately 1 cm, profiled the moving brash ice and the river stage through time. The brash ice keel was then inferred from the ice sail measurement, with a precision of approximately 20 cm.

1. Introduction

The ability to accurately profile ice thickness has military, commercial, and industrial applications (Yankielun, 1992). Radar profiling of river and ice dynamics is useful in assessing flood hazard, and water resources (Ferrick et al., 1995). Other important applications include monitoring ice motion to foresee potential damage to structures in and near the river, and evaluating the environmental impacts of breakup. This investigation uses a fixed, nadir looking, millimeter-wave (MMW) frequency modulated-continuous wave (FM-CW) radar to profile river stage and the elevation of broken ice floes, called brash ice, above the water surface. Brash ice, sometimes called rubble ice, consists of irregular sized and shaped slabs of broken river ice that have been forced together and rafted upon each other. **(Fig.1)**. Within the brash, the water surface of the river remains visible at random locations when viewed from above. The total ice thickness is the sum of the ice thickness above and below the water surface. One purpose of this measurement, using signal processing and statistical treatment, is to obtain the best estimate of the total brash ice thickness.

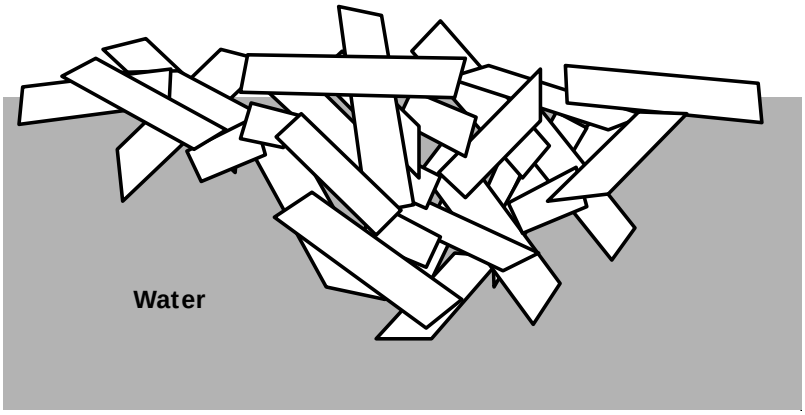

Fig . 1 – Representation of brash ice.

Prior use of pulse (Arcone and Delaney 1987, Chudobiak, et al. 1978) and FM-CW (Arcone, et al. 1997, Yankielun et al. 1993) radar to measure sheet ice thickness has been successful when the ice surface is fairly smooth. However, attempts to profile brash ice thickness have been compromised by the high radar reflectivity of the surrounding water and the indeterminacy of the subsurface readings caused by the roughness of the rubble. Daly et al. (1989) found that pulses centered near 50 MHz or less are required if penetration of more than a few meters is desired. However, all commercially available antennas mountable on a helicopter or on a bridge operate above 100 MHz. Daly et al. also found that any slope in the ice bottom profile greater than approximately 6˚ will cause energy reflected back through the water surface to refract into air too severely for detection. Therefore, the analysis of data from beneath the water line is not generally possible.

Previous radar profiling has been used in conjunction with manual measurements to estimate the thickness of subsurface brash ice. For example, C.R. Martinson et al. (1981) calibrated data from a subsurface radar through "ground truth" measurements. Daly et al. (1989) employed a helicopter-borne short-pulse radar to estimate rubble ice thickness from the mean freeboard height. We chose an FM-CW MMW radar based on the success of this radar in related studies (Arcone et al. 1997, Yankielun et al. 1992), and fixed this radar to a stable platform. Here, the radar was suspended over the Connecticut River from a bridge, to obtain range measurements to the ice and water surfaces below. The Ka-band (26.5 - 40 GHz) radar, with a spatial resolution of approximately 1 cm, was used to profile the brash ice freeboard and river stage as the ice moves past the radar antenna. The brash ice keel depth and total ice thickness **(Fig. 2)** can then be inferred from the radar-measured ice sail height with a precision of approximately 20cm.

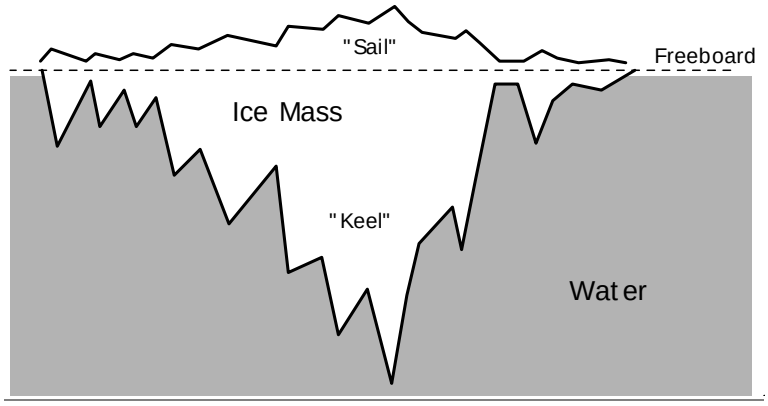

Fig 2 – Representation of components of a floating mass of ice.

River ice has a density of 0.9 g/ml and river water near the freezing point, has a density of 1.0 g/ml. Isostatic equilibrium of a block of ice floating in water will result in 90% of the volume of the ice submerged below the surface. Thus, if we are able to measure the "sail height" (height of the ice mass above the waterline), we can directly estimate the "keel depth" (depth of ice below freeboard) and the total ice thickness. **(Fig. 2)**

2. Measurement System Principles

The FM-CW principal is well known and has been described in depth by Botros and Oliver (1986); Stove (1992); Skolnick (1980), and Yankielun, et al. (1992). In a FM-CW system, **(Fig. 3)** a fixed amplitude, linearly frequency-swept sinusoidal signal is generated. The swept bandwidth of this signal is ΔF, and the sweep duration is t_{swp}, and is transmitted toward the target.

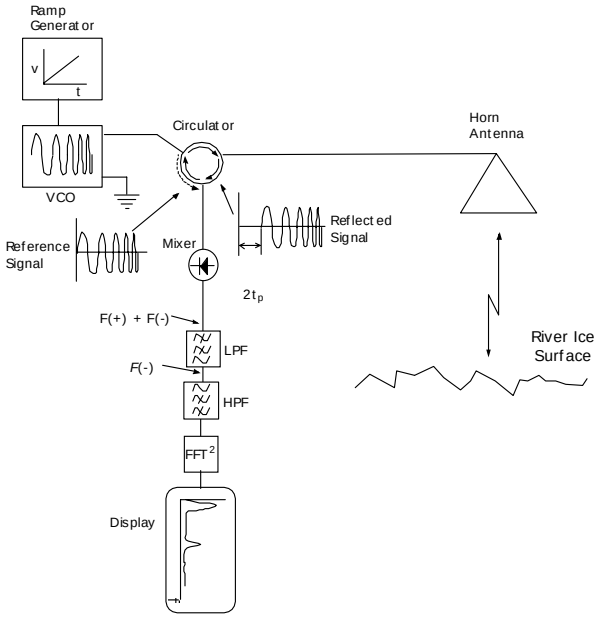

Fig. 3 – Block diagram of a FM-CW radar system.

We use a signal that is produced by a voltage-controlled oscillator (VCO) that can sweep bandwidths from hundreds of MHz to several GHz. The signal reflected from the target, delayed by the round-trip propagation time, $2t_p$, is mixed with a sample of the VCO output that is fed directly to the receiver with a minimal, but known delay. The mixing process produces sum, $F_{(+)}$, and difference, $F_{(-)}$, frequency signals. Low pass filtering is applied to retain only $F_{(-)}$. After Fourier transformation of $F_{(-)}$,one component, F_r is proportional to the range, R, of a target. The relationship between ΔF and F_r is

$$\frac{\Delta F}{t_{swp}} = \frac{F_r}{2t_p} \qquad [1]$$

R, and t_p can be related by

$$R = \frac{t_p c}{n}, \qquad [2]$$

where c = velocity of light in a vacuum (3×10^8 m/s) and n = medium index of refraction.

Substituting equation [1] into equation [2] and solving for R, we obtain

$$R = \frac{(F_r)(t_{swp})c}{2(\Delta F)(n)} \quad [3]$$

Thus, range to the surface of the brash ice mass and water surface can be determined by this radar technique. The time-series, filtered, mixer output of a FM-CW radar system is further processed by digital signal processing techniques, which include windowing, a fast Fourier transformation (FFT), and mathematical magnitude calculation. The result of this processing is a frequency power spectrum plot where range to a target is directly proportional to frequency. Thus spikes in the power spectrum represent the range and magnitude of the reflected radar signal from the water and ice targets. **(Fig. 4)**

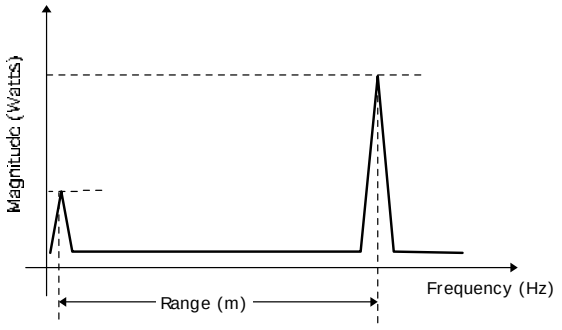

Fig. 4 – Arbitrary power spectrum illustrating radar signal magnitude and the relationship between range and frequency for an FM-CW radar where range (m) is directly proportional to frequency (Hz).

A mismatch of refractive indices exists at an interface of two different dielectric materials causes a fraction of the incident electromagnetic energy to be reflected back from the interface, while the complementary fraction of the energy is transmitted through the interface **(Fig. 5)**.

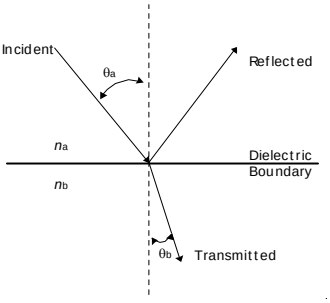

Fig. 5 – Illustration of reflection and transmission at a dielectric boundary. At an interface of two different dielectric materials, a fraction of the incident radar signal is reflected at the boundary and a fraction is transmitted through the boundary.

The fraction of the energy reflected back depends on the reflection coefficient. It is the dielectric contrast at an air/ice, air/water, or ice/water interface and respective reflection coefficients that make possible the measurement of river stage and ice thickness by electromagnetic methods. In general, the reflection coefficient, in terms of power, is defined as

$$\rho = \left| \frac{n_a \cos(\theta_b) - n_b \cos(\theta_a)}{n_a \cos(\theta_b) + n_b \cos(\theta_a)} \right|^2 \qquad [4]$$

where

n_a = refractive index of first material at the interface boundary.
n_p = refractive index of second material at interface boundary.
θ_a = incident angle, with respect to vertical.
θ_b = refractive angle, with respect to vertical.

with a normal (nadir) incident angle θ_a =0 and the associated normal refractive angle θ_b =0, the reflection coefficient for an arbitrary dielectric boundary discontinuity is given by a simplification of [4]:

$$\rho = \left| \frac{n_a - n_b}{n_a + n_b} \right|^2 \qquad [5]$$

Using the refractive indices of air (n_a =1), ice (n_i = 1.78) and water (n_w = 9) the reflection coefficients of the air/ice and air/water boundaries can be calculated. The air/ice boundary reflection coefficient is 0.08 and the air/water boundary reflection coefficient is 0.64. In decibels, the difference between the air/ice and air/water reflection coefficients is 9.08 dB. This significant difference permits a simple, automatic identification of both air/ice and air/water boundary reflections. All three possible conditions (i.e., open water, complete surface coverage by brash ice, and mixed open water and brash ice) can be detected, identified and displayed **(Fig. 6)**. In addition to the primary interest in using this phenomenon to obtain a freeboard baseline for ice thickness estimation, it can also be used to estimate the percent of open water versus ice cover, often called ice concentration.

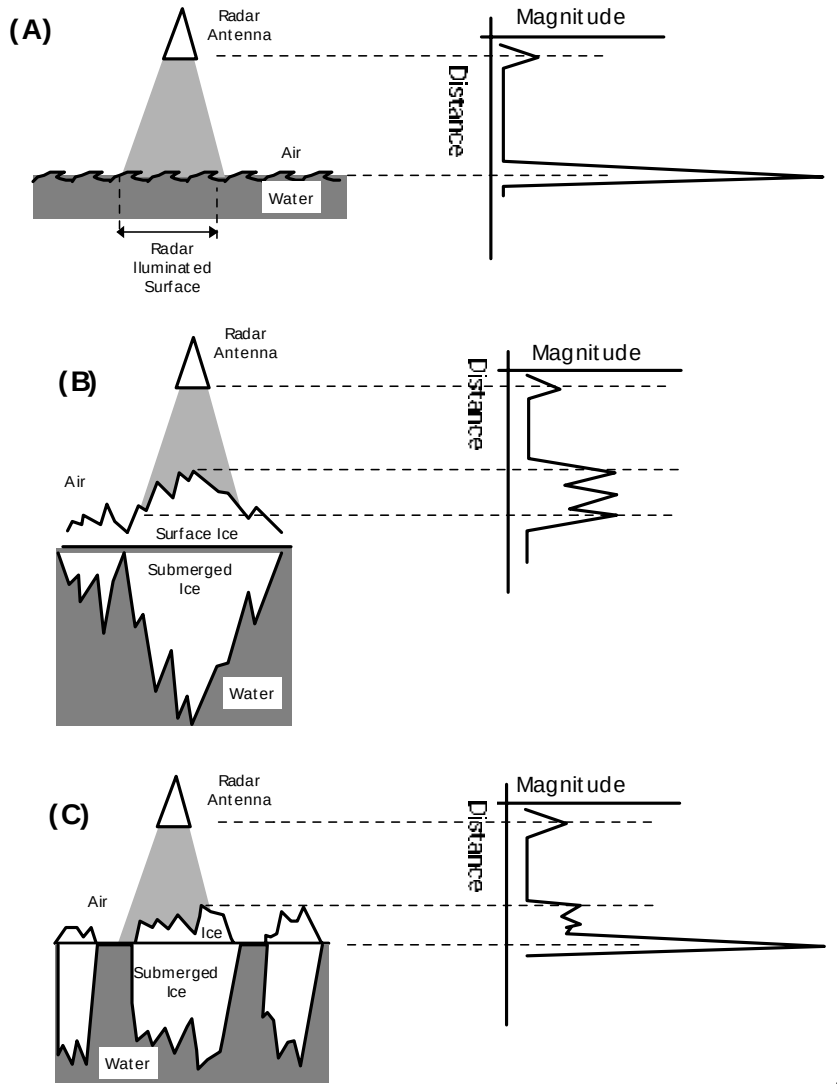

Fig. 6 – Typical radar waveforms for a variety of ice and water conditions. (A) Radar reflection from open water surface. (B) Radar reflection from dense brash ice. (C) Radar reflection from sparse brash ice.

The rate of change of river stage is very slow relative to the rate of change of the surface height of the brash ice above the waterline. Differences in these rates are typically several orders of magnitude. Even in densely packed brash ice there are frequent occurrences of open water. These open water patches produce high reflectivity radar returns relative to radar returns from the brash ice surface. The data from the radar are automatically processed in real time to reveal river stage and height of the brash ice above the water line (ice sail). From these data and the known buoyancy of ice, the depth of ice below the water line (ice keel) and total ice thickness can be estimated.

3. Signal Processing

Signal processing can be performed in real-time or in a post-acquisition mode using computer code written specifically for the purpose in a standard computer language (e.g., Fortran, C, Basic, etc.). Alternatively, the signal processing algorithm can be written, as it was in this case, using a graphical user interface (GUI) language where digital signal processing (DSP) modules can be interconnected to perform sequential signal processing functions. Here, the acquired real-time data is processed using an algorithm consisting of a window function, fast Fourier transform (FFT), magnitude calculator, a threshold detector, and a peak finder. **(Fig. 7)** The window function, FFT, and magnitude calculator functions are the standard elements of a FM-CW radar signal processor. The $F_{(\cdot)}$ signal from the radar output is transformed into a power spectrum by these signal processing elements. The power spectrum provides both frequency, proportional to radar range, and relative magnitude, proportional to reflection coefficient.

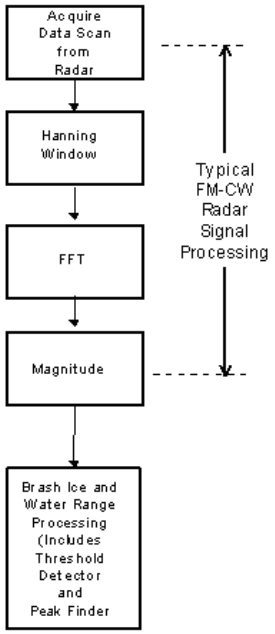

Fig. 7 – Radar signal processing block diagram.

For each of the combinations of river water and ice (open water, full ice cover, and mixed open water and ice cover) only two algorithm components are applied. The data are processed with the assumption that both ice and water surface reflections are always present. This permits a single signal processing algorithm data stream to be used. Again, as in the initial radar signal processing, Fortran, C, BASIC, or other programming language, as well as GUI based signal processing routines can be used for implementation.

In the case of a completely ice-covered river, **(Fig. 8A)**, a magnitude threshold is set at a level just above the noise floor of the spectral plot. This threshold is used to determine the highest elevation of the ice sail. The noise floor of the radar can be determined through calculation or by initially pointing the radar antenna towards the sky, but not towards the sun. The baseline of the resulting frequency power spectrum defines the noise floor. This calibration may be made at each system use, or stored for future reference.

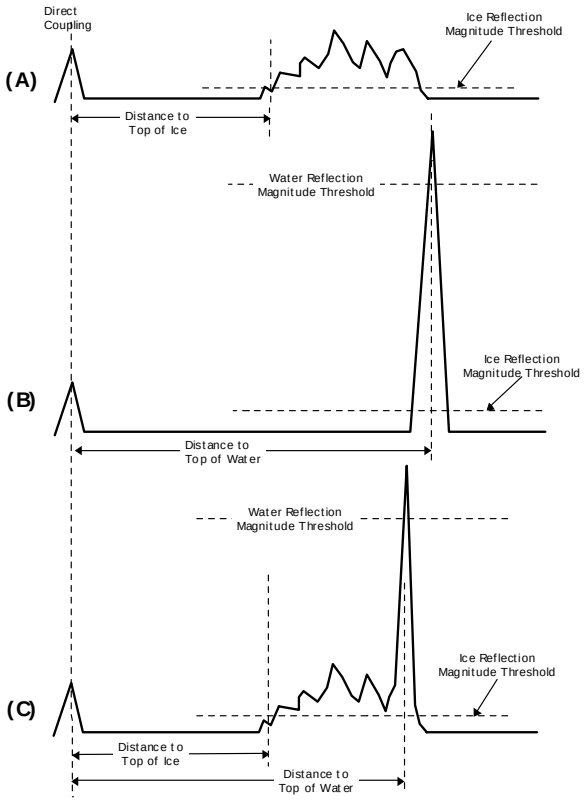

Fig. 8 – Decision thresholds and range determination. (A) Radar signal reflected from dense icepack. (B) Radar signal reflected from open water. (C) Radar signal reflected from sparse icepack.

In the case of open water, **(Fig. 8B)**, a magnitude threshold is set at an appropriate level, considerably above the noise floor and the maximum magnitude expected from brash ice radar reflection. This level can be set by pointing the radar perpendicular to open water (at the range expected for normal operation) and observing the peak magnitude of the radar reflection from the water surface. The baseline of the resulting frequency power spectrum defines peak amplitude of the water reflection. This calibration may be made at each system use, or stored for future reference. The water threshold can be set to some value below that maximum, say 60% – 80% of that peak value.

In the case of mixed open water and brash ice, the calibration practices and thresholds, described above, also apply. **(Fig. 8C)**

Fig. 9 illustrates the general signal processing methodology used for determining the range to the top of an ice sheet and to the water level. The position of the radar antenna **(Fig. 9A)** is illustrated as the vertical dotted line extending through the reflection peak occurring at the transition from the antenna mouth to space. This peak is called “direct coupling” and serves as a datum for range measurements to both the top of a brash ice mass and to the water surface. The

direct coupling peak in the radar waveform can be located using a peak detection algorithm or simply noted from an initial calibration of the system.

Fig. 9A also shows the two data decision threshold levels that have been previously established via the calibration methods discussed earlier. They are shown as two horizontal dotted lines running across the waveform. The upper dashed line represents the threshold level above which a peak magnitude would be indicative of a reflection from water. The lower dashed line represents a magnitude level, above the noise floor of the system, indicative of a radar reflection from the top of the brash ice pack.

In **Fig. 9B**, the spectral waveform is clipped at the water reflection decision threshold level. Clipping the lower magnitude spectral lines simplifies the process for the peak finding algorithm to locate the high magnitude spectral peak associated with a radar reflection off of the water surface. The search for the water surface reflection peak can be further simplified by bounding the distance range over which this peak may be expected to occur. The peak finding algorithm determines both the distance from the radar system and the magnitude of the water surface radar reflection. These values are stored for later use.

In **Fig. 9C**, the waveform of **Fig. 9A** is again processed to locate the leading edge of the radar reflection that represents a radar reflection from the highest point of the brash ice sail. The algorithm to detect the leading edge is relatively simple; a more complex algorithm that locates the first peak can be alternatively applied. Location of the first peak provides a more accurate estimation of ice rubble thickness than using the leading edge of the first peak. The first peak represents the true range to the ice surface whereas, the leading edge can occur a centimeter or two before the true maximum. Finding the first peak requires a more complex algorithm that both sets a threshold level and searches for the first peak appearance above that threshold.
To automate the calculation of maximum brash ice thickness, the current value of the highest point of the brash ice pack **(Fig. 9C)** is subtracted from the most recently measured distance from the radar to the water **(Fig. 9B)**. If the resulting value is zero, then it can be assumed that only open water is present within the microwave radar antenna beam pattern. If the resulting value is greater that zero, then there is brash ice present and simply multiplying this value of brash ice sail height by 10 gives an upper bound estimate of the total ice thickness. This process can be performed repeatedly to yield a continuous record of brash ice thickness. If a particular waveform contains no water reflection peak, then the most recent peak range value is used. Using this last-detected water reflection range is an appropriate technique since there is little variation in river stage over the time required for acquisition of multiple radar images. In typical cases, observable changes in river stage occur over minutes, whereas the repetition rate for acquisition of radar waveform is approximately 10 ms to 100 ms.

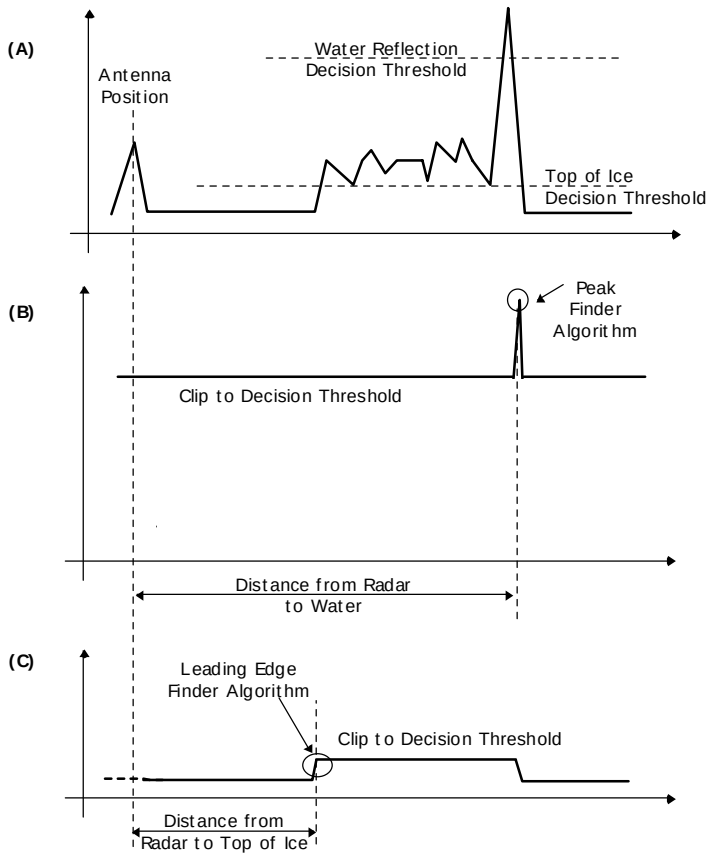

Fig. 9 – Determination of distance from radar antenna to the top of the ice and the water surface. (A) Raw radar signal showing amplitude thresholds. (B) Radar signal clipped at decision threshold for water reflection peak detection. (C) Radar signal clipped at decision threshold for top of icepack detection.

The use of decision thresholds and peak finding algorithms as applied to the radar spectral waveform are illustrated in Figures 10 and 11 for ice and open water, respectively.

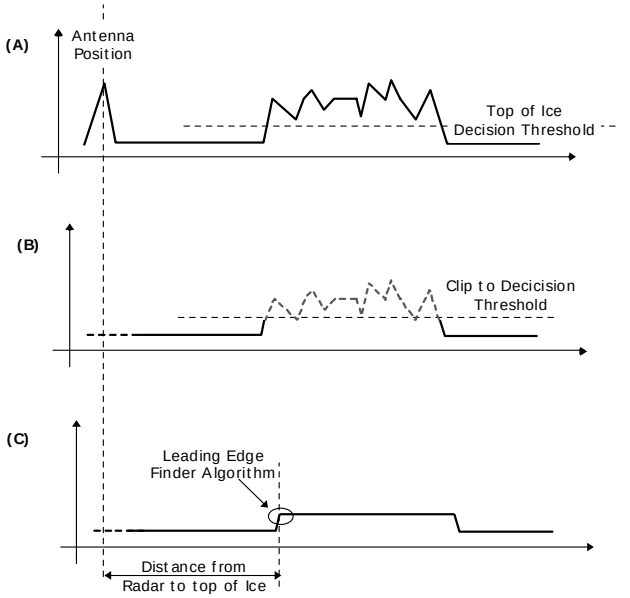

Fig. 10 – Determination of the distance from radar antenna to top of ice. (A) Raw radar signal showing top of ice decision threshold level. (B) Clipped signal. (C) Leading edge detector for locating top of icepack.

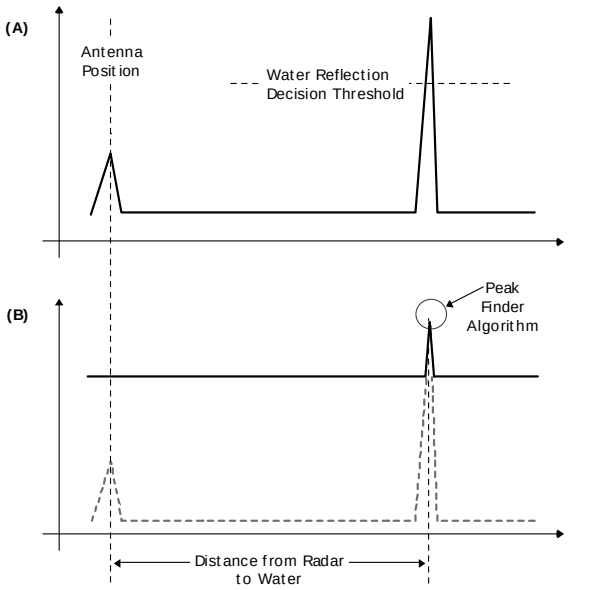

Fig. 11 – Determination of the distance from the radar antenna to the water surface. (A) Raw radar signal showing water reflection threshold. (B) Clipped radar signal for water surface range detection.

4. Results

The system we used was implemented using a generator-powered, high-resolution, MMW FM-CW radar system and a data acquisition equipped personal computer. The radar system was

nadir-mounted (perpendicular to the surface of the river) on a bridge spanning the Connecticut River, near Cornish, NH. and Windsor VT, during an ice breakup on 30 March 1993. The radar antenna was mounted approximately 6 m above the ice. The data collected were analyzed using digital signal processing software (DSP) incorporating the algorithms discussed earlier, which identified the peak reflection magnitude (return) from each radar scan. In this version of our processing software, multiple runs of the data set through the processing algorithm are required to establish and set the appropriate threshold levels.

Fig. 12 is representative of the dense brash ice cover encountered. **Fig. 13A** and **B** illustrate the output data from the radar system when there was dense brash ice covering the river. **Fig. 13A** is a 2500-second data record showing dense ice cover and sparse appearances of open water. **Fig. 13B** expands a 200 second data segment showing a detailed brash ice sail profile and few but sufficient water reflection data points to clearly indicate the upward trend in river stage.

Fig. 12 – Transition from moving sheet ice to compact, rafted, brash ice with little open water visible. Photo was taken only minutes after the start of ice motion at the bridge. View is from the Cornish-Windsor bridge looking upstream.

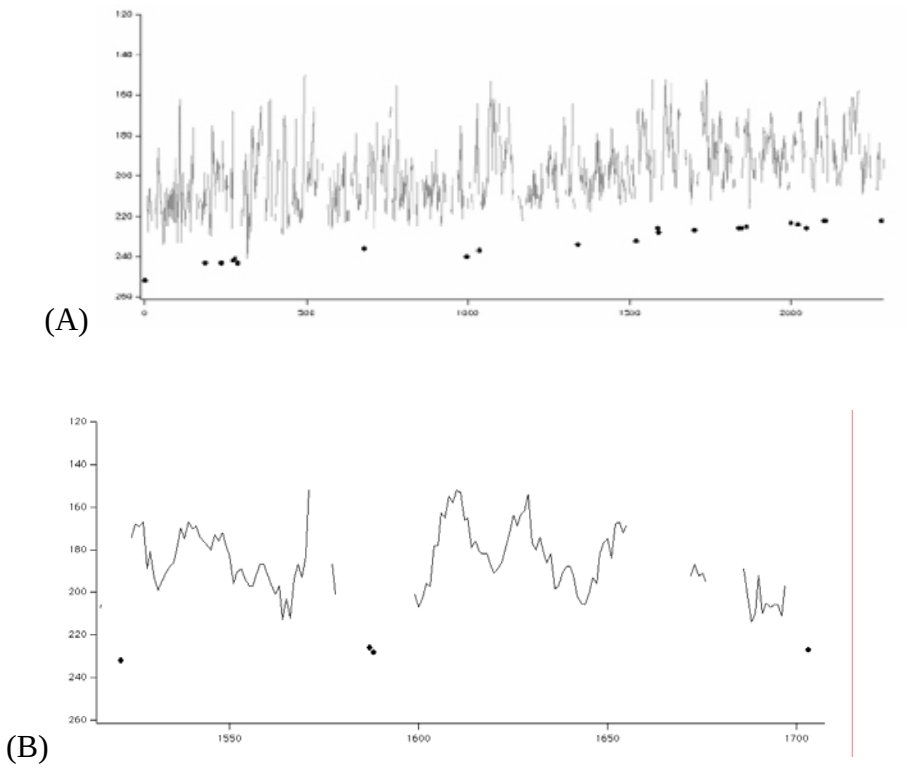

Fig. 13 – Output data from Ice Thickness Measuring Radar System for a Dense Ice Cover. Top graph (A) shows an extended time profile and lower graph (B) shows an expanded view of a shorter time segment. The line on each graph represents the profile of brash ice sail. Dots on the graphs represent distance from radar antenna to water surface. The vertical axis is centimeters and the horizontal axis is seconds.

Fig. 14 is representative of the thick, rafted brash ice and dispersed brash ice in largely open water encountered during this experiment. **Fig. 15A** and **B** represent the processed output data from the radar system where the ice is dispersed and sparse following the primary run. **Fig. 15A** is a 12000-second record showing the increase in river stage (black dots) and profiles (represented by the overlying line segments) of the occasional brash ice moving by our fixed position, downward-looking radar antenna. **Fig. 15B** is an expanded view of 500 seconds of the **Fig. 15A** record showing the profile of a single floe of brash ice passing beneath the antenna in approximately 100 seconds, surrounded by data points indicating river stage readings taken over open water. Here, few line segments indicate little ice present in mostly open water. Data give a nearly continuous profile of the river stage and an estimate of the percent of ice coverage of the river.

Fig. 14 -- Thick, rafted brash ice and dispersed brash ice in largely open water are both visible near the Cornish-Windsor bridge. These conditions occurred later in the breakup sequence as ice concentration was diminishing. View is from the left bank looking across and downstream.

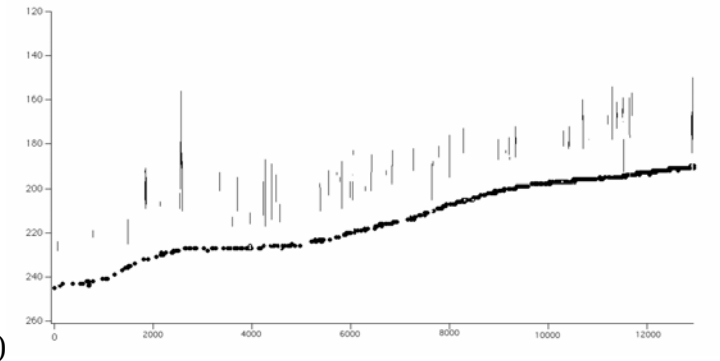

(A)

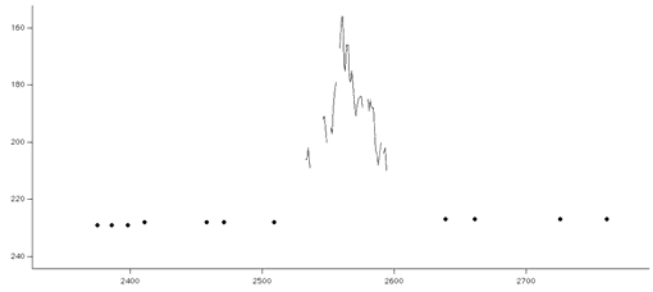

(B)

Fig. 15 -- Output data from Ice Thickness Measuring Radar System for a Sparse Ice Cover. Top graph (A) shows an extended time profile and lower graph (B) shows an expanded view of a shorter time segment. Line on graphs represent profile of brash ice sail. Dots on graph

represent distance from radar antenna to water surface. Vertical axis is centimeters and horizontal axis is seconds.

The data presented here can be further processed to provide much useful information to those concerned with river ice, flow dynamics, erosion and flooding. Given the ice sail height and river stage information acquired by this technique, ice keel depth and overall ice thickness can be estimated based on isostatic equilibrium. In addition to the graphical representation shown in the figures, a numerical representation of the thickness of the brash ice can be obtained, and simultaneously, river stage can be tracked in real time. When estimates of sail height and keel depth are combined with ice velocity data obtained from a Doppler radar such as that of Yankielun et al. (1996) ice discharge estimates and percent of river area covered by ice can also be determined. A video record enhanced the survey by detailing the open water area in two dimensions and by providing a simultaneous reference to support the final results of the study.

5. Conclusions

A high-resolution FM-CW MMW radar survey of river ice can provide a safe and accurate method of determining the ice conditions during breakup. As expected, increasing the fixed peak return and/or the amount of averaging decreases the amount of noise. Findings indicate that these two actions also vertically shift the data, corresponding to an increase in the estimated mean freeboard height. The accuracy of the subsurface brash ice profile estimate calculated from the radar depends on the choice of fixed peak return and averaging but is suitable for most applications.

Applications for this capability are monitoring ice breakup to predict flood hazard and possible bridge or environmental damage, estimating the forces applied by moving ice to piers and other riverine structures, and for collecting data to model ice and hydrodynamic processes.

While we placed the brash ice thickness measuring system on a fixed structure above the river with moving brash ice, it is conceivable that the same technique with little modification, could be used to estimate thickness of a stationary ice jam from a low, slow flying helicopter. Here, the reliance on ability to identify the radar reflections from open water are necessary to provide a baseline against which brash ice sail height can be measured. Our future effort will involve development of an automated statistical method to establish the decision thresholds used in processing the radar signal and optimally locate the top of the brash ice and water surface.

References

Arcone, S. A., Yankielun, N. E., and Chacho, E. F. Jr. (1997), "Reflection Profiling of Arctic Ice Using Microwave FM-CW Radar." *IEEE Trans. on Geoscience and Remote Sensing*, vol.35, no. 2, pp.436-443.

Botros, A.Z. and A.D. Oliver, 1986, Analysis of target response of FM-CW radar, IEEE Trans. Antennas and Propagation, Vol. AP-34, No. 4, 575-581.

Chudobiak, W.J., Gray, R., and Wight, J.S. (1978), “A nanosecond impulse X-band radar.” *Proc. of the IEEE*, 66(4): 523-524

Daly, S.F., and Arcone, S.A. (1989), “Airborne radar survey of a brash ice jam in the St. Clair River.” *CRREL Report 89-2*, U.S. Army Cold Regions Research and Engineering Laboratory, Hanover, NH.

Ferrick, M.G., Yankielun, N.E., and Nelson, D.F. (1995), “A Doppler Radar for Continuous Remote Measurement of River Ice Velocity.” *CRREL Report 95-21*, U.S. Army Cold Regions Research and Engineering Laboratory, Hanover, NH.

Martinson, C.R., and Dean, A.M. (1981),“Method for measuring brash ice thickness with impulse radar.” *CRREL Special Report 81-11*, U.S. Army Cold Regions Research and Engineering Laboratory, Hanover, NH.

Skolnick, M.L., *Introduction to Radar Systems*, McGraw-Hill, New York, 581 pp., 1980.

Stove, A.G., 1992, Linear FMCW radar techniques. IEE Proceedings, Vol. 139, No. 5, 343-350.

Yankielun, N.E., Ferrick, M.G., and Weyrick, P.B.1993,“Development of an airborne MMW FM-CW radar for Mapping River ice.” *CRREL Report 93-1*, U.S. Army Cold Regions Research and Engineering Laboratory, Hanover, NH .

Yankielun, N.E., Arcone, S.A., and Crane, R.K. 1992, “Thickness Profiling of Freshwater Ice Using a Millimeter-Wave FM-CW Radar”, *IEEE Trans. on Geoscience and Remote Sensing*; vol.80, no.5, pp.1094-1100.

Yankielun, N.E., et al, U.S. Patent No. 5,585,799, Microwave Doppler Radar System for Detection and Kinematic Measurements of River Ice, Dec., 17, 1996